Sustainable Food Technology

ROYAL SOCIETY OF CHEMISTRY

PAPER

View Article Online
View Journal

Cite this: DOI: 10.1039/d5fb00897b

Comparative study of sodium alginate films loaded with limonene and poly(limonene): interactions, properties, and functional activities

Matheus Milanez Leonetti,[ab] Vitor Emanuel de Souza Gomes,[a] Guilherme Frey Schutz,[b] Letícia Aliberti Galego Alves da Silva,[c] Liliana de Oliveira Rocha,[c] Roniérik Pioli Vieira[b] and Luís Marangoni Júnior *[a]

D-Limonene (LIM) is a terpene widely used as an additive in biopolymer-based active films, but its low thermal stability limits its applications. This study proposes using its thermally stable oligomer derivative, poly(limonene) (PLM), as an active component in sodium alginate (SA) films. PLM was synthesized *via* photopolymerization of LIM under mild conditions, yielding non-volatile oligomers with enhanced thermal stability. Scanning electron microscopy revealed a homogeneous surface distribution of the active oligomer in the films. Confirmatory analyses using Fourier-transform infrared spectroscopy and X-ray diffraction indicated reduced crystallinity after PLM incorporation. The addition of the active compounds did not significantly affect moisture content or water vapor permeability. While pure LIM exhibited inhibitory antimicrobial effects, none of the film solutions showed antimicrobial activity, likely due to low additive concentrations. Nonetheless, films with PLM demonstrated improved thermal stability and mechanical properties, with tensile strength increasing from 36 ± 3 MPa to 46 ± 5 MPa and elongation at break from 3.7 ± 0.8% to 14 ± 5% compared to the control films. Additionally, they presented a noticeable reduction in UV transmittance, indicating an improved UV light barrier. Films containing PLM also showed higher antioxidant activity than both the control and LIM films, with DPPH and ABTS scavenging effects of 7.8 ± 0.7% and 77 ± 16%, respectively. Overall, incorporating PLM is a promising strategy for utilizing citrus industry by-products, adding value to this natural compound while producing functional, biodegradable packaging materials with enhanced barrier and antioxidant features. Importantly, this work highlights the unexplored potential of PLM in SA films and provides new insights into how molecular structure affects film functionality. These advances contribute to the design of active packaging systems with improved stability and multifunctional performance.

Received 13th November 2025
Accepted 27th January 2026

DOI: 10.1039/d5fb00897b

rsc.li/susfoodtech

Sustainability spotlight

Packaging must be both circular and high-performing. We valorize a citrus by-product (D-limonene) by converting it *via* mild photopolymerization into poly(limonene) (PLM) and incorporating it into biodegradable sodium alginate films. Replacing volatile limonene with its oligomer enhances the material's thermal and mechanical properties, strengthens the UV-light barrier, and boosts antioxidant function without increasing moisture content or water vapor permeability. This molecular-design route upgrades renewable feedstocks into multifunctional materials, contributing to SDG 12 (Responsible Consumption and Production), SDG 9 (Industry, Innovation and Infrastructure), and SDG 13 (Climate Action).

1 Introduction

Food packaging plays a crucial role in protecting products against external agents, preventing exposure to microorganisms, light radiation, gases, and humidity.[1] To meet these requirements, synthetic polymer films are predominantly used due to their low permeability to gases and water vapor, favorable strength-to-weight ratio, flexibility, thermal stability, and economic viability.[2,3] Owing to their unique characteristics, the packaging industry has seen a rising demand for fossil-based polymers, driving research towards more sustainable alternatives. These efforts primarily focus on creating materials from renewable sources that balance functionality and efficiency.

Biopolymers stand out because of their renewable origin and biodegradability.[4] The most studied biopolymers for packaging

[a]Department of Food Engineering and Technology, School of Food Engineering, University of Campinas, 13083-862 Campinas, Brazil. E-mail: luismj@unicamp.br
[b]Department of Materials and Bioprocess Engineering, School of Chemical Engineering, University of Campinas, 13083-852 Campinas, Brazil
[c]Department of Food Science and Nutrition, School of Food Engineering, University of Campinas, 13083-862 Campinas, Brazil

include proteins and polysaccharides such as pectin,[5] chitosan,[6,7] chitin,[8,9] carrageenan,[2] starch[10,11] and sodium alginate,[12] have also been widely investigated due to their film-forming ability. Sodium alginate (SA) is a polysaccharide extracted from brown seaweeds, characterized by a linear chain structure composed of repeating α-L-guluronic and β-D-mannuronic acid residues linked *via* α-1,4-glycosidic bonds.[13] This versatile biopolymer has been extensively studied and applied across sectors such as pharmaceuticals,[14] food industry,[15] wastewater treatment,[16] and tissue engineering.[17] Its widespread application is due to its biocompatibility, biodegradability, non-toxicity, and high gelling capacity, making it a promising raw material for preparing films and coatings.[3,13] However, despite these advantages, SA-based films present limitations, including low mechanical strength, high water vapor permeability, reduced thermal stability, and high water solubility.[18]

One strategy to overcome these limitations is the incorporation of bio-based active additives. This approach improves physical, chemical, and functional properties, making films more suitable for food packaging applications.[19–22] Essential oils, in particular, have gained attention in recent years due to their contributions to food preservation and safety, while enhancing the physicochemical properties of the films.[23,24] Studies highlight the potential of active SA films in food preservation by reducing oxidation, providing antimicrobial protection, and blocking UV radiation.[25–28]

D-Limonene (LIM) is a cyclic monoterpene found in the essential oils of various citrus plants, such as lemon, orange, sage, and bergamot.[29,30] This compound is notable for its strong antioxidant and antimicrobial properties, which are vital for active packaging. LIM has been incorporated into different biopolymer films, including chitosan,[6] poly(itaconic acid)/starch,[11] poly(lactic acid),[31] and pectin.[5] However, its high volatility and thermal instability often lead to significant losses during film production and storage.[32] Poly(limonene) (PLM), an oligomer obtained from LIM through radical photopolymerization, has emerged as an alternative.[33] PLM exhibits higher thermal stability and lower volatility, while maintaining the bioactive properties of LIM. This makes it a more stable and effective additive for polymeric films, with the potential to overcome the limitations of monomeric LIM.[7] Furthermore, PLM demonstrates biocompatibility with biomaterials and does not show cytotoxic effects at concentrations of up to 5%, indicating its suitability for biomedical and food applications within this threshold.[11]

In this context, the present study aimed to produce and comparatively characterize SA-based active films incorporated with LIM and PLM. The objective was to evaluate the effects of different proportions of these additives on the films' morphology, structure, and mechanical and thermal properties. We also analyzed the interactions between the polymer matrix and the additives. Additionally, the study sought to assess the films' effectiveness in antioxidant and antimicrobial activities. This allowed a comparative analysis of the performance of films containing LIM *versus* those incorporating PLM. By addressing the limited understanding of polymerized LIM in SA matrices, this work fills a clear research gap. It provides a comprehensive evaluation of both structural and functional properties. This approach contributes to the development of multifunctional active packaging materials and informs the selection of additives for improved film performance.

2 Materials and methods

2.1 Materials

Sodium alginate (SA, purity ≥99%, with a 61 : 39 ratio of α-L-guluronic and β-D-mannuronic acids, respectively), D-limonene (LIM, purity ≥93%), *N*,*N*,*N*′,*N*″,*N*‴-pentamethyldiethylenetriamine (PMDETA, purity ≥99%), 2,2,2-tribromoethanol (TBE, purity ≥97%), benzophenone (BP, purity ≥99%), glycerol (GLI, purity ≥99%), and 2-[2-(2-hydroxyethoxy) propoxy]ethanol/Pluronic® F-127 (P, purity ≥99%) were purchased from Sigma-Aldrich (St. Louis, MO, USA). Dimethylacetamide (DMA, purity ≥99.5%) was bought from Vetec Química Fina Ltda. (Rio de Janeiro, RJ, Brazil).

2.2 Synthesis of poly(limonene)

PLM was synthesized *via* a radical polymerization through photoinitiation, following the methodology adapted from Oliveira *et al.*[33] and Santana *et al.*[5] The reaction was carried out using LIM as the monomer, TBE as the initiator, benzophenone as the type II photoinitiator, and PMDETA as the electron-donating amine, in a molar ratio of 100 : 1.7 : 1.7 : 8.5, respectively. DMA served as the solvent and the reaction mixture was prepared in glass flasks sealed with rubber septa and purged with nitrogen (N_2) for 10 minutes under magnetic stirring to remove oxygen. Subsequently, the flasks were placed in a box with eight UV lamps to maintain approximately constant light exposure (at 365 nm and an intensity of 4 mW cm^{-2}) for 6 hours at 40 °C. After the reaction, the resulting polymer was transferred to glass Petri dishes and dried in an oven at 45 °C for 48 hours to remove volatile components and residual monomer. Conversion was determined gravimetrically by comparing the polymer mass after reaction and dry steps to the initial monomer mass.

2.3 Preparation of limonene and poly(limonene) emulsions

For the incorporation of LIM and PLM into the films, separate emulsions of these compounds were prepared using Pluronic® F127 as a surfactant. The emulsions were formulated with 1 g of Pluronic® in each 100 mL of distilled water, which was stirred until complete solubilization and then subjected to sonication for 5 minutes. Subsequently, the required amount of LIM or PLM was added to the emulsion to achieve the desired concentration for the films (2.5% w/w or 5% w/w relative to the SA). Emulsification was performed using an Ultra-Turrax homogenizer (model T25 digital, IKA®-Werke GmbH & Co. KG, Staufen, Germany) operating at 20000 rpm for 3 minutes. Finally, the emulsions were sonicated with a high-intensity ultrasound device (Q Sonica, model Q700, USA) and stored at 5 °C until use.

2.4 Film preparation

The preparation of SA films was carried out using the casting method, as described in previous studies.[34] The composition of each formulation is summarized in Table 1. In brief, a control

film (SA) was prepared by dissolving SA (4% w/w) in distilled water, using glycerol (30% w/w relative to the biopolymer) as a plasticizer. The solution was homogenized with an Ultra-Turrax at 7000 rpm for 5 min. After complete dissolution, the SA solution was heated to 80 °C with continuous stirring for 15 min, followed by sonication under the same conditions to remove air bubbles. Subsequently, 50 g of the solution was poured into glass Petri dishes (145 mm diameter) and dried in an oven at 40 °C for 24 hours. For films containing LIM or PLM, the same procedure was applied, except that after heating, the solution was cooled to 40 °C before the addition of pre-prepared LIM or PLM emulsions. Final concentrations of 2.5% and 5% (w/w) were achieved in the film-forming dispersions. These mixtures were homogenized again using an Ultra-Turrax (7000 rpm for 5 minutes) before proceeding to the final casting and drying steps, as outlined for the control film. Additionally, control films containing only Pluronic® were prepared for comparison. After drying, the films were carefully removed from the dishes and stored at room temperature with controlled humidity.

2.5 Film characterization

2.5.1 Scanning electron microscopy (SEM). The morphological evaluation of the surface and cross-sectional microstructure of the films was performed using SEM, following the methodology described in Simon Maia *et al.*[35] Samples were pre-fractured in liquid nitrogen to obtain clean and sharp cuts and then coated with a thin layer of gold. The micrographs of the films were captured using a scanning electron microscope (SEM), model LEO 440i, equipped with an energy dispersive X-ray spectroscopy (EDS) detector, model 6070, both from LEO Electron Microscopy (Oxford, England). Images were acquired at an accelerating voltage of 15 kV, a current of 50 pA, and magnifications of 1000× for both surface and fracture analysis.

2.5.2 Visual and color analysis. The visual characterization of the films was carried out through photography to observe any perceptible changes in color, appearance, and homogeneity. The color analysis was performed following the methodology established by Kang *et al.*[36] Measurements were taken using a portable spectrophotometer (HunterLab, MiniScan XE 45/0-L, Reston, VA, USA), with a white background serving as the standard reference. For each formulation, five independent samples were analyzed, with measurements taken at three different points on each sample. This process yielded the parameters L^*, a^*, and b^*, corresponding to luminosity, the green/red coordinate, and the blue/yellow coordinate, respectively. The total color difference (ΔE) was calculated point-by-point, comparing each measurement of the formulation with that of the control film (SA), using the following eqn (1):

$$\Delta E = \sqrt{(L^* - L_0)^2 + (a^* - a_0)^2 + (b^* - b_0)^2} \quad (1)$$

where L^*, a^*, and b^* are the values for the sample, and L_0, a_0 and b_0 are the corresponding values measured for the control film.

2.5.3 Fourier transform infrared (FT-IR) spectroscopy. FT-IR analysis was performed to identify the functional groups present in the films, aiming to confirm the incorporation of LIM and PLM within the polymer matrix. The spectra were obtained using an FT-IR spectrometer (Anton Paar, Lyza 7000, Austria) in attenuated total reflectance (ATR) mode. Measurements were conducted over the spectral range of 4000–400 cm^{-1}, with a resolution of 4 cm^{-1}.

2.5.4 X-ray diffraction (XRD). X-ray diffraction (XRD) analysis was employed as a complementary technique to the other morphological assessments, following the methodology described by Schutz *et al.*,[37] to investigate the effects of incorporating LIM and PLM on the film structure. Diffraction patterns were obtained using an X'Pert-MPD X-ray diffractometer (Philips, Almelo, Netherlands), equipped with a Cu-Kα radiation source (λ = 1.54056 Å), operated at an acceleration voltage of 40 kV and a current of 40 mA. Measurements were performed over a 2θ range from 5° to 60°, with a scan rate of 0.0333° s^{-1}, corresponding to a step size of 0.04° every 1.2 seconds.

2.5.5 Thermogravimetric analysis (TGA). The thermal behavior and degradation profile of the films were evaluated using TGA and DTG analyses, following the methodology described by Barbosa *et al.*,[6] to assess the impact of different additive concentrations on the thermal stability of the films. Samples of 10 mg of each film were placed in crucibles of 70 μL volume and heated from 25 °C to 600 °C at a rate of 20 °C min^{-1} under a nitrogen flow of 50 mL min^{-1}. The analyses were performed using a TGA-50 thermogravimetric analyzer (Shimadzu, Kyoto, Japan).

2.5.6 Moisture content (MC) and water vapor permeability (WVP). The moisture content (MC) of the films was determined *via* gravimetric analysis in triplicate for each formulation, following the methodology described by Vianna *et al.*[11] The mass of each sample, cut into squares measuring 2 cm × 2 cm, was measured using a digital analytical balance, model Adventurer AR2140 (Ohaus, Parsippany, USA), with a resolution of 0.1 mg. Measurements were taken before and after drying in an

Table 1 Composition (%, w/w) of the film formulations

Materials	SA	SA/P	SA/P/LIM2.5%	SA/P/LIM5%	SA/P/PLM2.5%	SA/P/PLM5%
Sodium alginate (SA)	4.00	4.00	4.00	4.00	4.00	4.00
Glycerol	1.20	1.20	1.20	1.20	1.20	1.20
Pluronic® (P)	—	0.40	0.40	0.40	0.40	0.40
Limonene (LIM)	—	—	0.10	0.20	—	—
Poly(limonene) (PLM)	—	—	—	—	0.10	0.20
Water	94.80	94.40	94.30	94.20	94.30	94.20

oven at 105 °C for 24 hours to determine the initial mass (m_0) and final mass (m_1) of the films. The moisture content was calculated using eqn (2):

$$\mathrm{MC}\ (\%) = \frac{m_0 - m_1}{m_0} \times 100 \quad (2)$$

To determine water vapor permeability (WVP), in triplicate for each formulation, the films were cut into circles with an area of 50 cm^2, and the thickness of each sample was measured at 10 different points using a Mitutoyo Absolute digital comparator, model 543-450B (Mitutoyo Mexicana S.A. de C.V., Mexico), with a resolution of 1 μm. Subsequently, 25 g of anhydrous calcium chloride (PA) was placed into capsules, which were covered with the film, sealed with a silicone ring, and closed tightly. The capsules with the samples were then placed in a climate chamber (PROLAB, model SSCCU, São Paulo, Brazil) maintained at 25 °C and 75% relative humidity. At intervals of 1 hour, the capsules were removed, and their mass was measured using a precision analytical digital balance (Marte, model AY220, Minas Gerais, Brazil) with a resolution of 0.1 mg. The values of the water vapor transmission rate (WVTR) in g m^{-2} s^{-1} were obtained from the slope of the "mass increase × time" curve, according to the ASTM E96/E96M[38] standard. Based on this, the WVP in g m^{-1} s^{-1} Pa^{-1} was calculated using eqn (3).

$$\mathrm{WVP} = \frac{\mathrm{WVTR} \times e}{p_s \times \mathrm{RH}} \quad (3)$$

In eqn (3), the term e corresponds to the average thickness of the sample (m), p_s is the water vapor saturation pressure at 25 °C (3168 Pa), and RH is the relative humidity of the chamber (75% = factor 0.75), considering that the relative humidity inside the capsule is zero.

2.5.7 Thickness of the films. The film thickness was determined following the ISO-4593[39] standard. Measurements were taken at five different points on each sample using a Mitutoyo Absolute digital dial gauge, model 543-450B (Mitutoyo Mexicana S.A. de C.V., Mexico), with a resolution of 1 μm. This procedure was performed on three different film samples for each formulation to obtain an average value.

2.5.8 Mechanical properties of the films. To evaluate the mechanical properties of the SA films with the incorporation of LIM and PLM into their matrix, tensile tests were performed in quintuplicate for each formulation, following the ASTM D882[40] standard. The elastic modulus (EM), tensile strength (TS), and elongation at break (EB) were measured using a universal testing machine (EZ-LX HS, Shimadzu, Kyoto, Japan), with samples 15 mm in width and 100 mm in length. The tests were conducted using a 2 kN load cell, an initial grip separation of 50 mm, and a crosshead speed of 12 mm min^{-1}.

2.5.9 Light transmission. The light barrier properties of the films were evaluated through light transmission analyses to understand the influence of LIM and PLM on this property within the SA polymer matrix. Transmittance measurements were performed in triplicate for each formulation using a UV-Vis spectrophotometer (Specord 210, Analytik Jena, Germany), operating at a scanning speed of 120 nm min^{-1} over the wavelength range of 200 to 800 nm, following the ASTM E1348[41] standard.

The UV blocking efficiency, eqn (4), of the films was determined by integrating the spectral transmittance, $T(\lambda)$ (%), across the corresponding wavelength ranges of UVC (200–280 nm), UVB (280–315 nm), and UVA (315–400 nm), assuming a uniform spectral weighting. The average transmittance for each band was calculated using the trapezoidal numerical integration method. For comparative purposes, a total UV blocking value (200–400 nm) was also computed. This approach provides a quantitative assessment of the film's ability to prevent UV radiation transmission across the different spectral regions.

$$\mathrm{UV\ blocking}(\%) = 100 - \frac{\int_{\lambda 1}^{\lambda 2} T(\lambda)\mathrm{d}\lambda}{\int_{\lambda 1}^{\lambda 2} \mathrm{d}\lambda} \quad (4)$$

2.5.10 Antioxidant activity. The antioxidant activity of the samples was assessed using the DPPH radical scavenging assay, following the method described by Barbosa *et al.*[6] For this, 45 mg of each formulation, in triplicate, were incubated with 3 mL of ethanolic DPPH solution (0.1 mmol L^{-1}) for 30 minutes at room temperature and protected from light. The absorbance was measured at 517 nm using a UV-Vis spectrophotometer (Kasuaki, IL-592-LC-BI model, Tokyo, Japan). The percentage of antioxidant activity for each sample was determined using eqn (5), where $\mathrm{Abs_{DPPH}}$ represents the absorbance of the DPPH solution and $\mathrm{Abs_{extract}}$ is the absorbance of the sample:

$$\mathrm{DPPH\ scavenging\ effect}(\%) = \left(\frac{\mathrm{Abs_{DPPH}} - \mathrm{Abs_{extract}}}{\mathrm{Abs_{DPPH}}}\right) \times 100 \quad (5)$$

Similarly to the DPPH assay, the antioxidant activity of the films was also evaluated using the ABTS radical cation scavenging activity. In triplicate, 15 mg of each formulation were incubated with 5 mL of aqueous ABTS solution for 1 hour at room temperature and in the absence of light. Absorbance measurements were taken with a UV-Vis spectrophotometer. The antioxidant activity (%) was calculated using eqn (6), where $\mathrm{Abs_{ABTS}}$ represents the absorbance of the ABTS solution and $\mathrm{Abs_{extract}}$ is the absorbance of the sample:

$$\mathrm{ABTS\ scavenging\ effect}(\%) = \left(\frac{\mathrm{Abs_{ABTS}} - \mathrm{Abs_{extract}}}{\mathrm{Abs_{ABTS}}}\right) \times 100 \quad (6)$$

2.5.11 Antimicrobial activity. The antimicrobial activity of the films was evaluated based on an adaptation of the methodology described by Akachat *et al.*,[42] using filter paper as a support for applying the film-forming solutions. The tested microorganisms included the bacterium *Bacillus cereus* due to its spoilage potential and ability to cause foodborne diseases, and the fungi *Aspergillus niger* and *Paecilomyces variotii*, both recognized as major food spoilage agents.[43–45] For the antibacterial assay, *B.*

cereus was cultured on Nutrient Agar (NA), at 30 °C for 48 hours, after which the bacterial growth was harvested and suspended in 1% peptone water. The suspension was adjusted to a concentration of 10^8 CFU mL^{-1}. Subsequently, the surface of Petri dishes containing NA was inoculated with 0.1 mL of the bacterial suspension. For the antifungal assay, *A. niger* and *P. variotii* strains were pre-cultured on Potato Dextrose Agar (PDA) at 25 °C for 7 days. After this period, suspensions of 10^7 spores mL^{-1} were prepared using 1% Tween 80 for each fungus, and these suspensions were spread onto plates containing the same medium.

The plates were prepared under three conditions: without any treatment (positive control, PC), in the presence of an antimicrobial agent (inhibition control, IC), and with the film-forming solutions of the formulations: SA, SA/P, SA/P/LIM 2.5%, SA/P/LIM 5%, SA/P/PLM 2.5%, and SA/P/PLM 5%. In the ICs, ciprofloxacin was used for *B. cereus*, and pure LIM (20 μL) for *A. niger* and *P. variotii*. For the other conditions, 20 μL of the respective film solution was deposited onto a sterile filter paper disc (6 mm diameter), placed at the center of each plate after microbial inoculation. The cultures were incubated at 30 °C for 24 hours for bacteria and at 25 °C for 7 days for fungi. After incubation, the plates were photographed for qualitative assessment of inhibition zones around the discs. All tests were performed in triplicate for the controls and each film formulation.

2.5.12 Statistical analysis. All experiments with quantitative results were conducted in triplicate or quintuplicate, and their outcomes were expressed as mean values with standard deviation. Statistical analysis was performed using SAS software (Statistical Analysis System), version 9.4, from SAS Institute Inc. (Cary, NC, USA). An analysis of variance (ANOVA) was used, followed by Tukey's *post hoc* test for mean comparisons, considering a significance level of $p < 0.05$.

3. Results and discussion

3.1 Visual and morphological analysis by SEM

As observed in Fig. 1, overall, the SA films exhibited a uniform and homogeneous appearance, with no signs of pores or bubbles. The formulations SA, SA/P, SA/P/LIM2.5%, and SA/P/LIM5% appeared more translucent and colorless. Meanwhile, the films SA/P/PLM2.5% and SA/P/PLM5% showed a yellowish hue, attributed to the presence of PLM, with its intensity increasing proportionally to the concentration. The absence of macroscopic spots or heterogeneous regions suggested that PLM was homogeneously dispersed within the SA matrix at the evaluated concentrations.

SEM images allow direct visualization of the films' microstructure, which strongly affects properties such as water vapor permeability and mechanical characteristics. The surface micrographs presented in Fig. 1 reinforced the films' predominantly uniform microstructure. However, particulate dispersions were visible, especially in the samples containing PLM, likely resulting from partially emulsified additive during film preparation.

The incorporation of LIM and PLM altered the surface morphology, creating cavities suggestive of successful incorporation of these additives. In the SA/P/PLM5% formulation, although the overall visual aspect remained uniform (Fig. 1k), a faint dark spot was identified on the surface micrograph. This may result from accumulated PLM, suggesting that its dispersion may have been less efficient at higher concentrations. In contrast, the SA/P/PLM2.5% formulation did not show such irregularities, corroborating previous findings on PLA/PBAT films with PLM.[46]

SEM images of the cross-sections (Fig. 1b, d, f, h, j and l) revealed the presence of some undissolved crystals, particularly in samples with LIM and PLM. This may be related to the hydrophobic nature of these compounds, which reduces their compatibility with hydrophilic biopolymers such as SA. Although such crystals have not been reported in other studies, the literature acknowledges the low compatibility of LIM and PLM with hydrophilic matrices.[7,37] Microcracks and holes were observed mainly in the cross-section of films containing LIM, especially SA/P/LIM5%, likely resulting from the volatilization of the oil from the polymer matrix. This behavior has been previously reported by Schutz *et al.*[37] and Toledo *et al.*[46] For films with PLM, less pronounced surface porosity and indications of oil droplets were observed, particularly at higher concentrations. Earlier studies with PLM reported more intense visual spots on the surface than those observed in the present study.[7,37] This reinforced that, despite occasional agglomerates, PLM achieved satisfactory homogeneity within the SA matrix. Overall, both surface holes and internal porosity detected in the cross-section suggest that LIM and PLM were dispersed as particles of various sizes throughout the film matrix.

3.2 Color analysis

The color of packaging materials can significantly influence consumer preferences and is associated with their ability to block visible and ultraviolet radiation, thereby aiding in the protection of photosensitive compounds. Table 2 summarizes the effects of incorporating LIM or PLM on the color parameters of SA-based films. Overall, films containing PLM exhibited significant changes ($p < 0.05$) compared to the other formulations. The chromatic coordinates a^* and b^* were significantly higher ($p < 0.05$) than those of the control and LIM-containing films, highlighting the characteristic yellowish hue associated with the oligomer. This observation has also been visually noted by Gonçalves *et al.*[7] and Vianna *et al.*[11] Brightness (L^*) was also significantly reduced ($p < 0.05$) in the samples with PLM, due to their appearing more opaque and darker, which tended to hinder light transmission through the film.[47] Finally, the overall color difference (ΔE) was significant ($p < 0.05$) between PLM films and the other formulations, especially at higher PLM concentrations, due to its inherent yellow coloration, as seen in Fig. 1.

3.3 FT-IR and XRD analysis

FT-IR analysis was conducted to identify potential interactions between SA and the added active compounds (LIM and PLM). In all analyzed films (Fig. 2a), bands were observed around 3240 cm^{-1}, 1596 cm^{-1}, and 1407 cm^{-1}, corresponding,

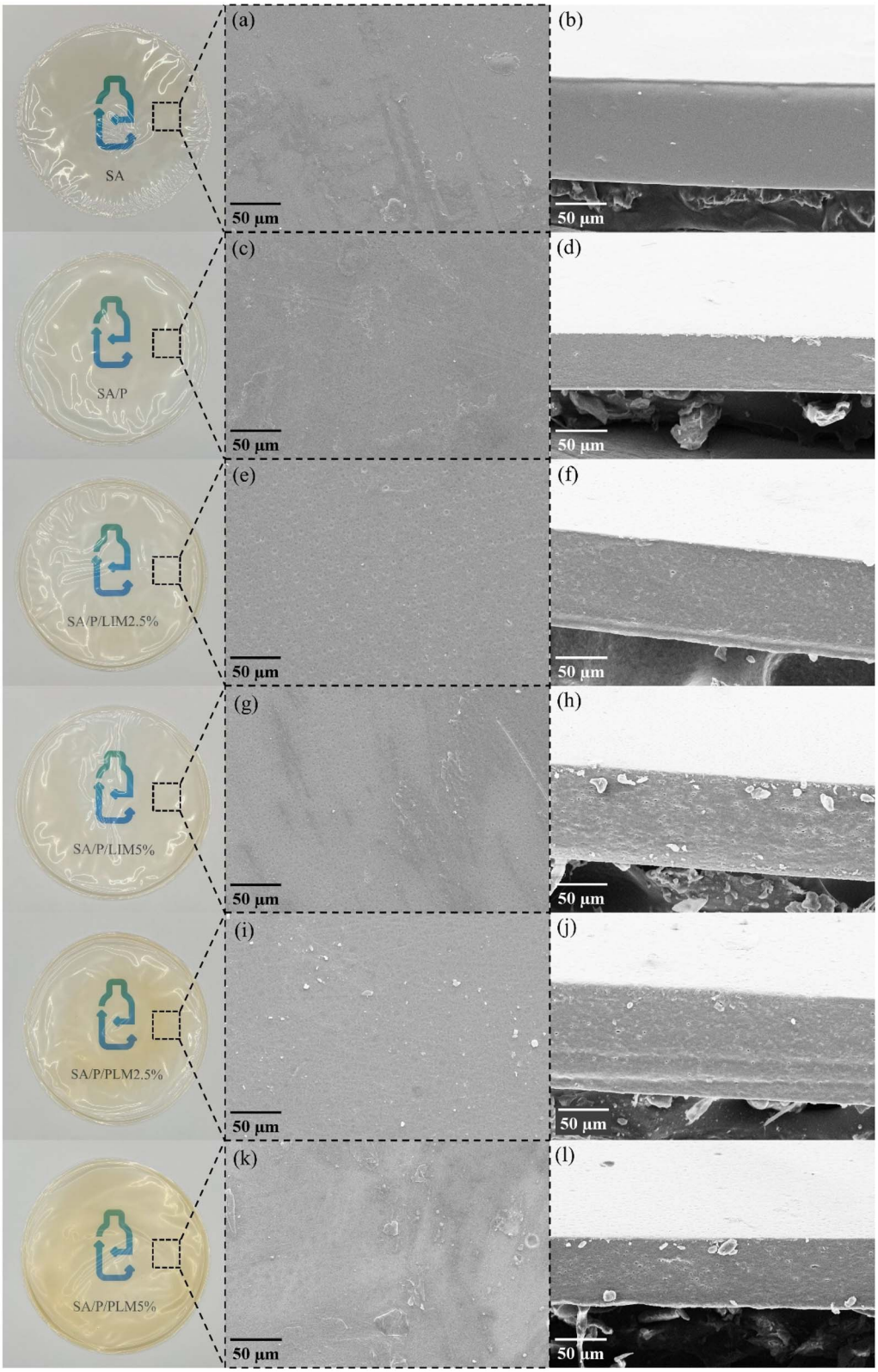

Fig. 1 Photographs of the films (left) and micrographs of the surfaces and cross-sections at 1000× magnification (right) of the films SA (a and b), SA/P (c and d), SA/P/LIM2.5% (e and f), SA/P/LIM5% (g and h), SA/P/PLM2.5% (i and j), and SA/P/PLM5% (k and l).

respectively, to the hydroxyl group (–OH) and the asymmetric and symmetric vibrations of the carboxylate groups ($–COO^-$). These bands are characteristic of the SA structure and have been reported in previous studies on this polysaccharide.[48,49] No significant changes were detected in the spectra of films containing LIM and PLM compared to the control. This lack of

Table 2 Color properties of the SA-based films[a]

Film	L^*	a^*	b^*	ΔE
SA	89.48 ± 0.54[a]	1.40 ± 0.17[b]	−0.46 ± 1.46[d]	0.00 ± 0.00[d]
SA/P	88.88 ± 0.85[a]	1.41 ± 0.11[b]	1.97 ± 2.09 [cd]	3.16 ± 1.93 [cd]
SA/P/LIM2.5%	89.46 ± 0.76[a]	1.34 ± 0.07[b]	2.58 ± 1.86[c]	3.35 ± 2.11[c]
SA/P/LIM5%	88.87 ± 0.54[a]	1.36 ± 0.05[b]	3.72 ± 1.28[c]	4.37 ± 2.23[c]
SA/P/PLM2.5%	85.67 ± 1.48[b]	1.59 ± 0.25 [ab]	11.91 ± 3.26[b]	12.95 ± 4.13[b]
SA/P/PLM5%	83.09 ± 1.93[c]	1.79 ± 0.50[a]	18.87 ± 4.05[a]	20.37 ± 5.37[a]

[a] L^*: brightness; a^*: green/red coordinate; b^*: blue/yellow coordinate; ΔE: total color difference. Values are presented as mean ± standard deviation. Different letters (a–d) in the same column indicate a significant difference between samples according to the Tukey test ($p < 0.05$).

alteration may be related to the low additive concentrations and to overlapping bands of SA and the additives themselves, as observed in other studies involving the addition of LIM or PLM in starch-based[37] and chitosan-based films.[6]

Nevertheless, a reduction in the intensity of the band associated with the hydroxyl group (around 3240 cm^{-1}) was noticeable upon the addition of LIM and even more pronounced with PLM. This change was likely linked to a decrease in the number of free hydroxyl groups in the SA chains, possibly due to the hydrophobic nature of LIM and PLM, which restricts the exposure or interaction of these groups.[7,50] Additionally, peaks near 842 cm^{-1} were observed, corresponding to the bending vibrations of the C–H bonds in the PLM ring. An increased intensity of the peak at 2888 cm^{-1} was also noted, attributed to the stretching vibrations of –CH and $–CH_2$ groups in the chains of the surfactant Pluronic® F-127.[51] Furthermore, a small peak around 1343 cm^{-1} appeared in the SA/P film, with its intensity increasing alongside the concentration of LIM and PLM. This band can be associated with the bending vibration of the O–H bond, characteristic of Pluronic® F-127, as previously reported in surfactant studies.[51,52]

Fig. 2b shows the diffractograms of the control films and those incorporated with LIM or PLM. The X-ray profiles indicate that all films exhibited a predominantly amorphous nature. Characteristic amorphous halos were observed at approximately $2\theta \approx 15.5°$ and $2\theta \approx 21.5°$, which are typical of SA.[48] The incorporation of LIM and PLM appeared to reduce the intensity of both halos, especially the one at 15.5°. These findings are consistent with the results reported for starch-based biocomposite films containing the same additives.[37]

3.4 Thermal stability of the films

Fig. 3 shows the TGA and DTG curves of the SA-based films. Table 3 presents the onset degradation temperature (T_{onset}), the maximum degradation temperature (T_{max}), and the mass loss percentages for each thermal event identified in the analysis. Three thermal events were observed within the examined temperature range, except in the control SA formulation, which exhibited only the first two events.

The first thermal event was similar across all formulations and was associated with the evaporation of moisture adsorbed within the films.[48,53] This behavior is consistent with the moisture content (MC) values previously obtained (Fig. 4a). In addition to water, films containing LIM also exhibited evaporation of the terpene itself within the 50–120 °C range.[6] The

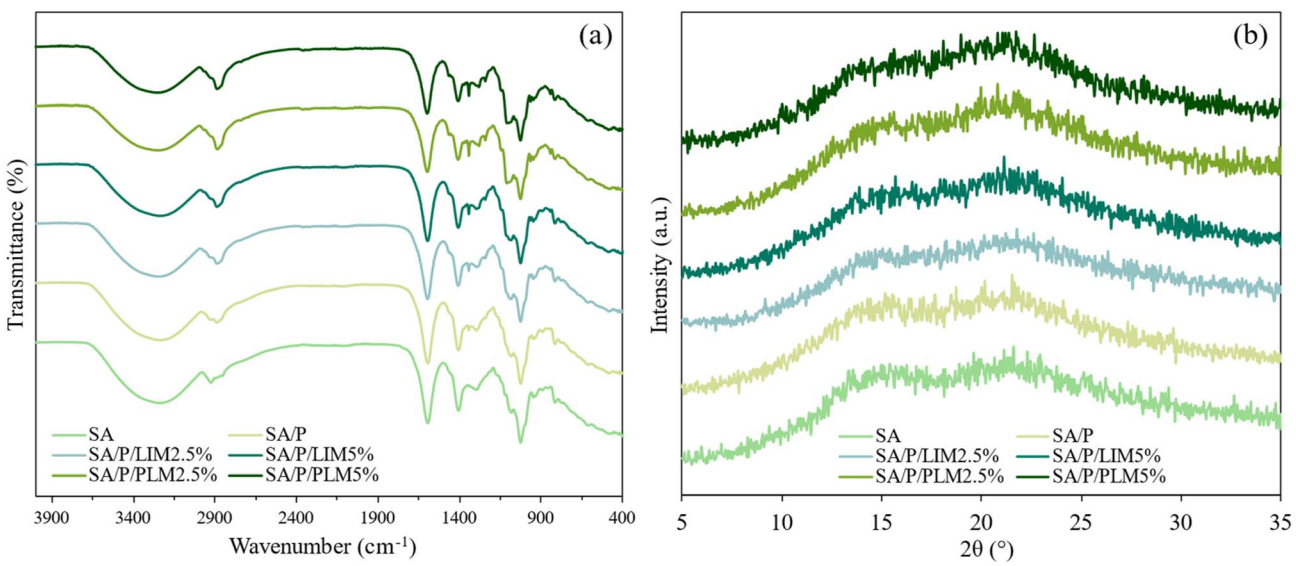

Fig. 2 FT-IR spectrum (a) and X-ray diffraction (XRD) profile (b) of the SA, SA/P, SA/P/LIM2.5%, SA/P/LIM5%, SA/P/PLM2.5%, and SA/P/PLM5% films.

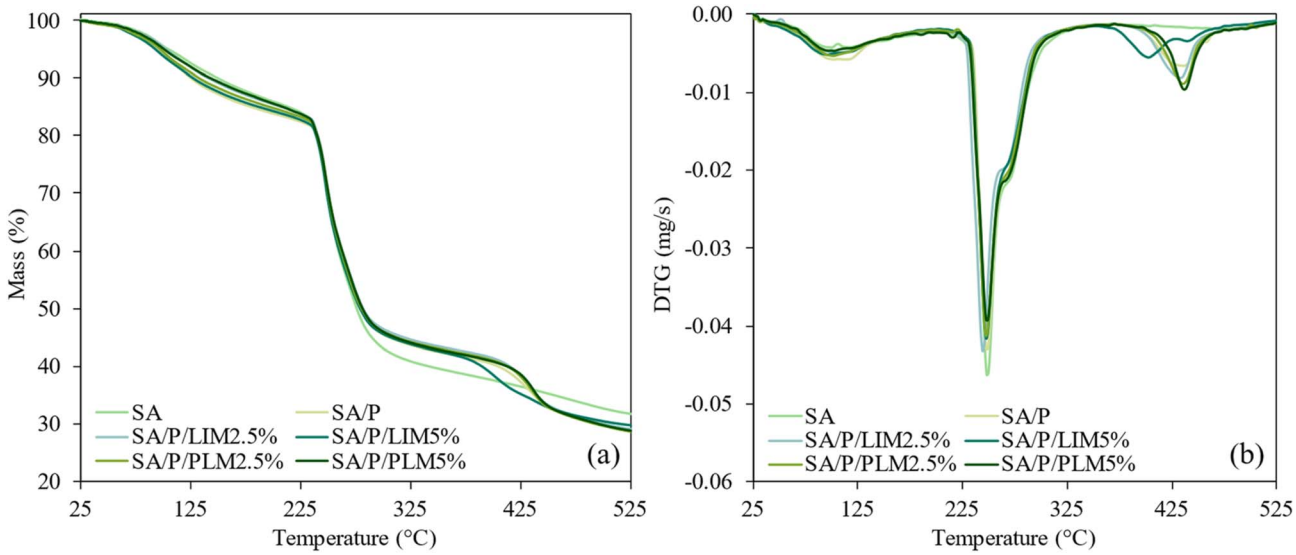

Fig. 3 TGA (a) and DTG (b) curves for the films SA, SA/P, SA/P/LIM2.5%, SA/P/LIM5%, SA/P/PLM2.5%, and SA/P/PLM5%.

second event corresponded to the degradation of the SA polymer chains, primarily involving the cleavage of glycosidic bonds and decarboxylation of protonated carboxyl groups.[48,54] Thermal degradation of incorporated glycerol also occurred during this interval.[7] In formulations with PLM, degradation of the oligomer began at approximately 255 °C.[11,46] The third event is likely related to the thermal decomposition of Pluronic® F-127, which generally occurs in the 350–420 °C range.[55–57] This explains its absence in the control SA formulation.

During the second thermal event, T_{max} values remained close to 248 °C across all formulations. However, a reduction of about 6% in mass loss was noted for the films containing LIM and PLM compared to the others. These results suggest a slight enhancement in thermal stability upon the incorporation of the additives, although no statistically significant differences were observed. Similar findings were reported by Gonçalves *et al.*,[7] who observed improved thermal stability in chitosan films incorporated with PLM. Among the formulations tested, the SA/P sample displayed the lowest mass loss at this stage, with approximately a 6.5% reduction compared to the control SA film.

In the third thermal event, the T_{onset} values were higher for films containing PLM, with a trend of increasing T_{onset} corresponding to higher PLM concentrations. T_{max} values remained at around 436 °C for nearly all samples. An exception was the SA/P/LIM5% sample, which exhibited a degradation peak at 402.62 °C, roughly 30 °C lower than the others. Overall, mass loss during this final event was relatively consistent across the formulations, ranging from 14.5% to 15.7%.

3.5 Moisture content (MC) and water vapor permeability (WVP)

According to the results shown in Fig. 4a, films containing LIM exhibited the lowest MC values among the analyzed samples. However, these reductions were not statistically significant ($p > 0.05$), as no formulation differed significantly from each other. The MC ranged from approximately 11% to 14%. Generally, the incorporation of terpenes such as LIM and its derivatives is expected to increase film hydrophobicity. This occurs because the additives reduce the availability of polar groups capable of interacting with water,[6] which is expected to decrease the MC. In this context, the lack of a significant reduction may be attributed to the low concentrations of LIM and PLM used. This indicated that the amount of additive incorporated was insufficient to influence the film's hygroscopicity.

Packaging films play a crucial role in protecting food by acting as barriers to moisture transfer. In this context, WVP is

Table 3 Onset degradation temperature (T_{onset}), maximum degradation temperature (T_{max}), and mass loss of the films SA, SA/P, SA/P/LIM2.5%, SA/P/LIM5%, SA/P/PLM2.5%, and SA/P/PLM5%

	1st thermal event			2nd thermal event			3rd thermal event		
Film	T_{onset} (°C)	T_{max} (°C)	Mass loss (%)	T_{onset} (°C)	T_{max} (°C)	Mass loss (%)	T_{onset} (°C)	T_{max} (°C)	Mass loss (%)
SA	65.54	100.39	14.184	240.66	248.29	47.250	—	—	—
SA/P	64.32	107.70	16.200	241.15	248.87	40.860	411.61	436.12	14.992
SA/P/LIM2.5%	67.83	108.43	14.768	239.72	247.70	41.291	413.09	436.85	15.700
SA/P/LIM5%	62.31	101.85	15.426	238.03	248.14	41.050	386.49	402.62	14.586
SA/P/PLM2.5%	70.39	102.43	14.734	238.40	247.85	41.764	417.20	435.39	15.490
SA/P/PLM5%	67.02	102.73	14.272	239.03	248.43	42.562	421.49	436.71	15.109

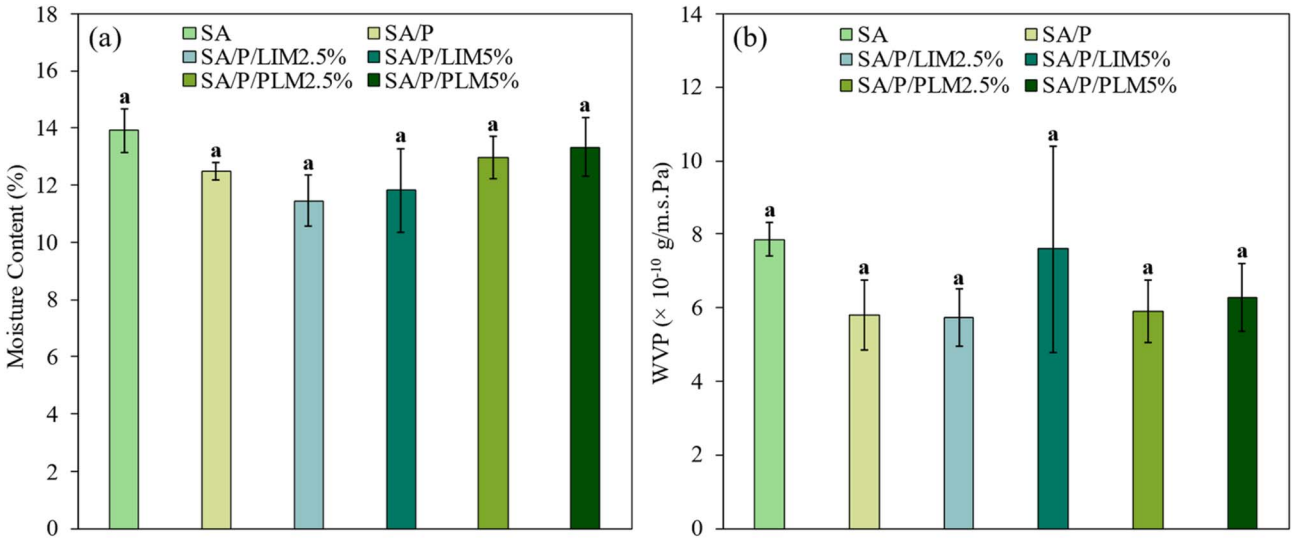

Fig. 4 MC (a) and WVP (b) for the films SA, SA/P, SA/P/LIM2.5%, SA/P/LIM5%, SA/P/PLM2.5%, and SA/P/PLM5%. Different letters (a–c) indicate significant differences between samples according to the Tukey test ($p < 0.05$).

a key parameter for evaluating the efficiency of the material's hydrophobic barrier under specific thermal conditions.[58] The WVP values, depicted in Fig. 4b, were slightly lower for formulations supplemented with LIM and PLM, including the SA/P sample. However, similar to the MC results, this reduction was not statistically significant ($p > 0.05$) at the concentrations tested. Reducing WVP is desirable in food packaging applications, as limiting moisture permeation between the product and the environment is fundamental for maintaining food quality.[6,59] In this regard, hydrophobic compounds such as essential oils and their derivatives can decrease moisture permeation rates.[60] This occurs by filling the spaces between polymer chains and increasing the tortuosity of the water vapor diffusion path.[58] These findings highlight the potential of the tested additives, suggesting that higher concentrations could be explored to achieve more significant improvements in the barrier properties of SA-based films.

3.6 Film thickness

As shown in Fig. 5a, the average thickness of the SA and SA/P films was 103.2 ± 26.5 μm and 96.5 ± 10.2 μm, respectively. A slight increase in thickness was observed with the incorporation of LIM and PLM. However, these variations were not statistically significant ($p > 0.05$), possibly due to the low additive concentrations. Except for the SA/P/LIM5% sample, all other formulations containing the additives exhibited thickness values similar to the control film, ranging from approximately 100 to 110 μm. This increase in thickness could be associated with an expansion in the spacing between SA chains, likely caused by the intercalation of LIM and PLM molecules, which hampers the regular packing of the polymer matrix.[6,11]

3.7 Mechanical properties

Given the importance of good mechanical performance in coating films to ensure packaging integrity and durability,[6] the results indicated that the incorporation of LIM and PLM at the evaluated concentrations (2.5% and 5%) did not negatively affect the films' mechanical properties, as shown in Fig. 5. The elastic modulus (EM), tensile strength (TS), and elongation at break (EB) for the SA films were 1572 ± 114 MPa, 36 ± 3 MPa, and 3.7 ± 0.8%, respectively. The SA/P films exhibited values of 1704 ± 349 MPa, 46 ± 3 MPa, and 7 ± 2%, respectively. Compared to the control films, EM showed no significant changes ($p > 0.05$) with increasing concentrations of LIM and PLM. This suggests that the films maintained their rigidity even after the addition of the active compounds (Fig. 5b).

Regarding the TS (Fig. 5c), formulations containing lower concentrations of additives showed higher values than the SA film, but were similar to the SA/P film, around 45 MPa. The SA/P/PLM5% formulation did not differ significantly ($p > 0.05$) from any other formulation, with a TS of 38 ± 4 MPa, close to that of the SA film. Meanwhile, the SA/P/LIM5% formulation had the lowest TS among all samples (36 ± 8 MPa), being statistically similar ($p > 0.05$) only to SA/P/PLM5%. The EB values (Fig. 5d) for the SA/P/LIM2.5% and SA/P/PLM2.5% samples (13 ± 5% and 14 ± 5%, respectively) were significantly higher ($p < 0.05$) than that of the control SA film (3.7 ± 0.8%), despite the high variability in the data. The EB value for the SA/P/PLM5% formulation was 13 ± 2%, which was statistically higher ($p < 0.05$) than those of the SA and SA/P/LIM5% films, but similar ($p > 0.05$) to those of SA/P/LIM2.5% and SA/P/PLM2.5%.

These findings diverge from the general trend reported in the literature, where incorporating essential oils or their hydrophobic derivatives into polysaccharide-based films typically reduces TS. This reduction is generally due to the disruption of polymer–polymer interactions and phase separation, resulting in heterogeneous and mechanically weakened structures.[60] Interestingly, in the present study, films containing Pluronic® F-127, whether combined with SA alone or in the presence of LIM or PLM, exhibited enhanced TS compared to the SA control. This suggests that the surfactant may play

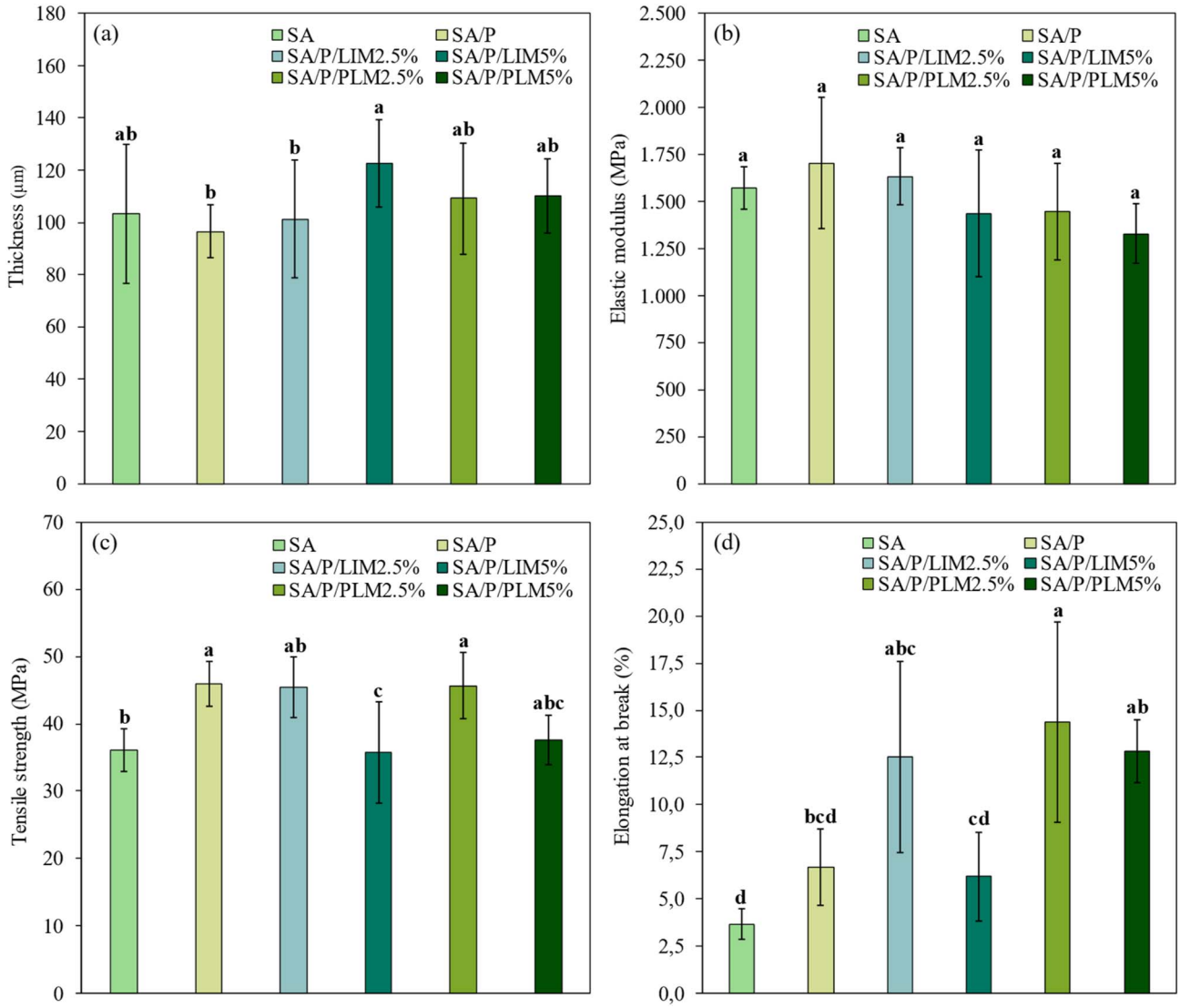

Fig. 5 Thickness (a), elastic modulus (b), tensile strength (c), and elongation at break (d) of the films SA, SA/P, SA/P/LIM2.5%, SA/P/LIM5%, SA/P/PLM2.5%, and SA/P/PLM5%. Different letters (a–d) indicate significant differences between the samples according to the Tukey test ($p < 0.05$).

a structuring role, promoting better dispersion of hydrophobic compounds and reducing interfacial tension, thereby improving film homogeneity. Furthermore, in the case of PLM, the presence of polar terminal groups may have enabled secondary interactions, such as hydrogen bonding or dipole–dipole interactions, with the SA chains. This likely contributed to a more cohesive and reinforced network, as similarly observed by Gonçalves *et al.*[7] in chitosan films.

The increase in EB values may be related to the plasticizing effect of essential oils, which enhances film flexibility.[61,62] Additionally, Pluronic® F-127 may also have contributed to the increased TS and EB by promoting cohesion and adhesion between SA chains. Similar effects have been reported for polycaprolactone-based films, where Pluronic® improved their mechanical properties.[63] In summary, based on TS and EB parameters, the films containing the additives demonstrated performance equal to or better than the control film, highlighting their potential for application as biodegradable packaging materials.

3.8 Light transmission

The transmittance spectra of the films (Fig. 6) and the quantitative UV-blocking data (Table 4) consistently demonstrate the superior light-shielding performance of PLM-incorporated formulations. Statistical analysis confirmed significant differences among all samples across the UVA, UVB, UVC, and total UV ranges. In the UVA region (315–400 nm), PLM films achieved the highest blocking efficiencies, 91.3 ± 1.0% for SA/P/PLM5% and 88.2 ± 3.2% for SA/P/PLM2.5%. These values were markedly higher than those of LIM films (77–79%) and far superior to the control matrices SA and SA/P (38.5% and 74.5%). The same trend was observed for UVB and UVC regions, where PLM films reached efficiencies above 95%, statistically surpassing all other samples. LIM-based films displayed intermediate behavior, while the control films exhibited the poorest performance, confirming the reinforcing role of both additives, especially PLM.

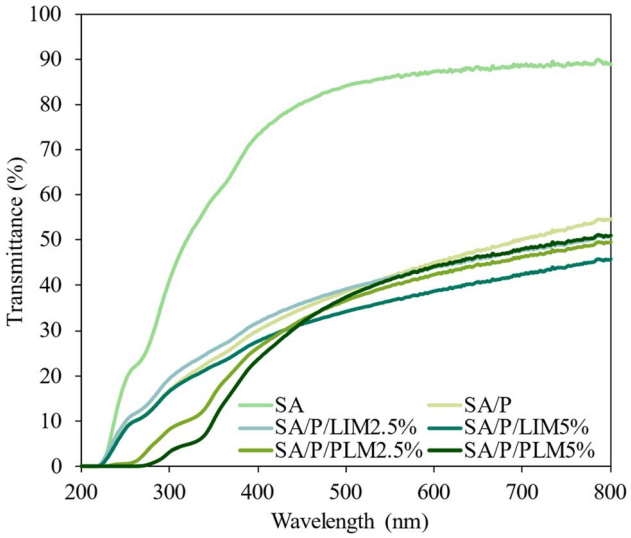

Fig. 6 Transmittance (%) graph as a function of wavelength (nm) for the films SA, SA/P, SA/P/LIM2.5%, SA/P/LIM5%, SA/P/PLM2.5%, and SA/P/PLM5%.

This promising UV light barrier performance can be attributed to the molecular structure of PLM, which is highly responsive to light absorption at shorter wavelengths. This behavior results from the preserved endocyclic π-bond originating from LIM during the polymerization process.[7] Regardless of concentration, PLM films provided greater UV protection than LIM films. Their darker, opaque appearance likely also contributed to this effect, contrasting with the more translucent look of the LIM samples. These properties are crucial for packaging applications, as UV radiation accelerates oxidative processes in foods, especially in lipids, which can reduce nutritional quality and shelf life.[64]

In the visible range (400–800 nm), films with LIM and PLM also reduced light transmittance. In contrast, the control SA film presented higher transmittance. Film thickness, as shown in Fig. 5a, may have influenced these results. For instance, the SA/P/LIM5% formulation was the thickest among the analyzed films, which likely contributed to its improved light-blocking performance. Variations in thickness may affect the light barrier properties of the films.[6]

The UV barrier efficiency achieved with PLM incorporation is consistent with values reported for high-performance biopolymer-based films (Table 5). The near-complete blocking in the UVC/UVB region observed for the SA-based films is comparable to results obtained using carbon nanomaterials, modified biopolymers, and inorganic nanoparticles.[65–69] In these systems, UV shielding efficiencies are remarkably high, which is generally attributed to the presence of aromatic or conjugated structures and/or inorganic nanoparticles. These components act as efficient UV absorbers and scattering centers, reducing light transmittance through electronic transitions, reflection, and multiple scattering of high-energy radiation.[65–69]

Notably, while most high-performance barriers in Table 5 exhibit minimal transmittance in the UVB/UVC range, the films with PLM maintained a visible light transmittance of 44.2%. This is significantly higher than that observed for the TiO_2 system.[69] These findings indicate that PLM provides a light-shielding capability similar to conventional additives while maintaining moderate translucency in biopolymeric matrices.

3.9 Antioxidant activity

Fig. 7a illustrates the antioxidant activity of the films when in contact with the free radical DPPH. Incorporating antioxidant properties into food packaging materials is essential to maintain product quality and extend shelf life.[70] The employed method is based on the neutralization of nitrogen-centered radicals of DPPH by hydrogen-donating antioxidant compounds. This reaction converts DPPH into its reduced form, DPPH-H.[7]

The control formulations (SA and SA/P) and SA/P/LIM2.5% exhibited the lowest antioxidant activities, all below 4%. The best-performing films were SA/P/LIM5% and SA/P/PLM5%. Although SA/P/LIM5% did not differ significantly from the control SA ($p > 0.05$), the SA/P/PLM5% formulation showed a statistically higher activity ($p < 0.05$). When comparing films loaded with LIM and PLM at the same concentration, the results for PLM were higher, although not significantly different ($p > 0.05$). This trend may be related to the structure of PLM, which contains repeating LIM units with endocyclic double bonds that favor stabilization of DPPH radicals.[7,11]

The low concentration of PLM used, combined with an exposure time of only 30 minutes, may have limited the release of the active compound. This could explain the lack of significant differences observed. Previous studies with higher PLM concentrations in biopolymeric matrices, such as pectin[5] and poly(itaconic acid)/starch,[11] reported more pronounced

Table 4 UV-light blocking efficiency (%) of the films SA, SA/P, SA/P/LIM2.5%, SA/P/LIM5%, SA/P/PLM2.5%, and SA/P/PLM5%[a]

Film	UVA (%)	UVB (%)	UVC (%)	Total UV (%)
SA	38.5 ± 3.8^{c}	60.9 ± 5.4^{e}	88.1 ± 3.2^{d}	62.3 ± 3.9^{c}
SA/P	74.5 ± 0.4^{b}	83.1 ± 0.3^{d}	93.9 ± 0.4^{b}	83.8 ± 0.5^{b}
SA/P/LIM2.5%	78.6 ± 2.4^{b}	86.7 ± 1.7^{cd}	96.0 ± 1.0^{b}	86.3 ± 3.0^{b}
SA/P/LIM5%	77.5 ± 5.3^{b}	85.6 ± 4.1^{c}	95.1 ± 1.8^{b}	85.5 ± 3.4^{b}
SA/P/PLM2.5%	88.2 ± 3.2^{ab}	95.5 ± 0.8^{b}	99.4 ± 0.2^{a}	94.0 ± 1.4^{a}
SA/P/PLM5%	91.3 ± 1.0^{a}	98.6 ± 0.2^{a}	99.9 ± 0.0^{a}	95.5 ± 0.5^{a}

[a] Values are presented as mean ± standard deviation. Different letters (a–e) in the same column indicate a significant difference between samples according to the Tukey test ($p < 0.05$).

Table 5 Comparison of UV-light transmittance at 280 nm (UVB) and 600 nm (visible light) for the SA/P/PLM5% film and high-performance biopolymer-based composites[a]

Base material	UV agent	Transmittance at 280 nm	Transmittance at 600 nm	References
Alginate	PLM	0.7%	44%	This work
Cellulose nanofiber	MXene	<1%	~58%	65
Chitin	Surface modification (Hantzsch reaction)	<1%	~88%	66
κ-carrageenan	Lignin	<1%	~60%	67
Gellan/Xanthan	ZnO	<1%	~70%	68
PVA/CNC	TiO_2	<1%	~7%	69

[a] For a fair comparison, the selected data from the literature[65–69] correspond to formulations with additive concentrations similar to those used in this work (typically 1–10 wt%). The specific samples were chosen based on their optimized balance between maximum UV-blocking efficiency and maintaining adequate visible light transparency.

antioxidant activities. Therefore, higher concentrations of PLM and/or longer contact times with radicals could enhance the antioxidant efficacy of the SA films, allowing sufficient time for active compound release.

In the ABTS assays, which are presented in Fig. 7b, films incorporated with PLM demonstrated excellent antioxidant activity. Control and LIM-based formulations showed activities between 10% and 30%. In contrast, SA/P/PLM2.5% and SA/P/PLM5% reached values close to 40% and 80%, respectively. These results indicate a significant difference ($p < 0.05$) between PLM and LIM in scavenging ABTS radicals. The better performance of PLM may be related to its higher thermal stability and lower volatility compared to LIM, which reduce the loss of active compounds through evaporation or degradation.[7,46] Furthermore, SA/P/PLM5% performed significantly better ($p < 0.05$) than SA/P/PLM2.5%, suggesting that increasing the additive concentration directly enhances the films' antioxidant activity.

In this assay, the films were exposed to ABTS radicals for 1 hour. This longer exposure likely provided enough time for the diffusion and release of active compounds into the medium, which may explain the superior antioxidant performance compared to the DPPH test. Additionally, the presence of the surfactant Pluronic® F-127 may also have contributed to this effect. Its hydrophilic poly(ethylene oxide) segments facilitate the formation and release of micelles containing the hydrophobic additives. This mechanism improves dispersion in the aqueous ABTS solution and increases the accessibility of antioxidant compounds to the radicals, thereby enhancing scavenging activity. These findings are consistent with previous results obtained from chitosan films containing LIM, where the influence of exposure time was similarly observed.[6] Therefore, longer testing periods with DPPH could reveal even higher antioxidant activities in films with PLM at the studied concentrations.

3.10 Antimicrobial activity

The microbial culture plates with the tested microorganisms under different conditions are shown in Fig. 8. None of the evaluated formulations demonstrated antimicrobial activity, as evidenced by the absence of inhibition zones around the

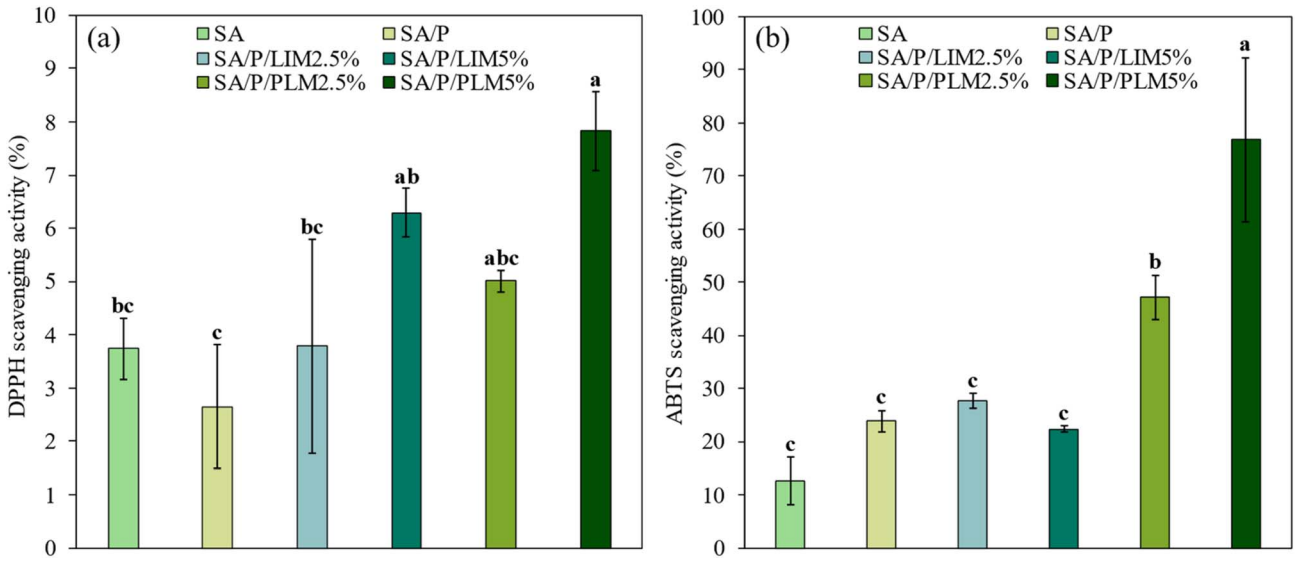

Fig. 7 Antioxidant activity against DPPH radicals (a) and ABTS radicals (b) for the films SA, SA/P, SA/P/LIM2.5%, SA/P/LIM5%, SA/P/PLM2.5%, and SA/P/PLM5%. Different letters (a–c) indicate significant differences between the samples according to Tukey's test ($p < 0.05$).

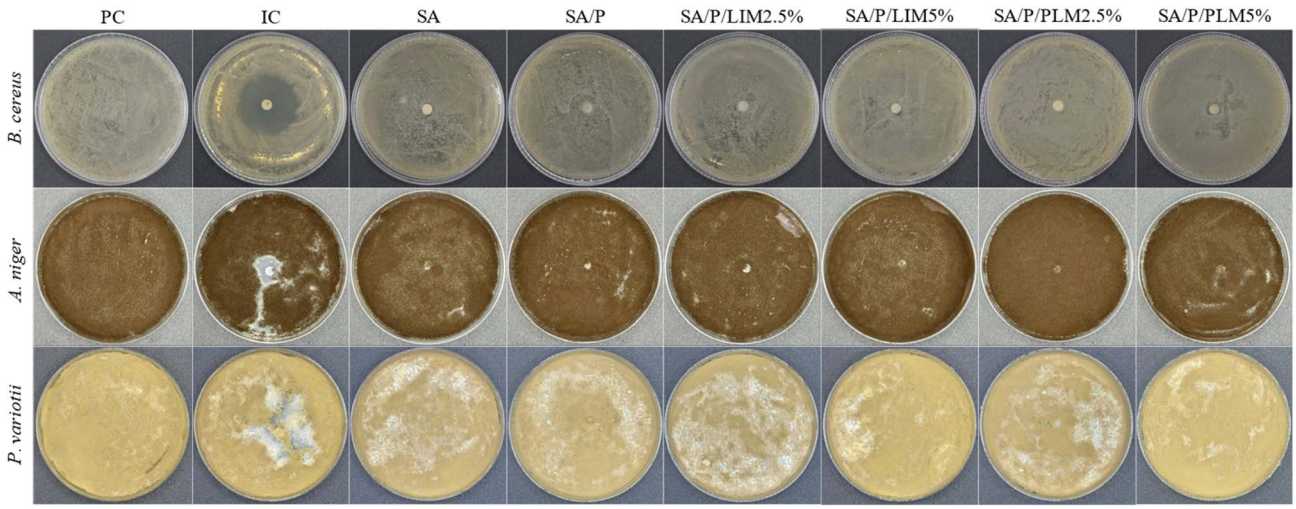

Fig. 8 Photographs of the culture plates containing *Bacillus cereus* (*B. cereus*), *Aspergillus niger* (*A. niger*), and *Paecilomyces variotii* (*P. variotii*) under different conditions: no treatment (positive control – PC), in the presence of an antimicrobial agent (inhibition control – IC), and in contact with the film solutions of the formulations SA, SA/P, SA/P/LIM2.5%, SA/P/LIM5%, SA/P/PLM2.5%, and SA/P/PLM5%.

samples containing the film solutions. All formulations appeared visually similar to the positive control (PC). In contrast, the inhibition control (IC) showed clearly visible antimicrobial activity: the antibiotic inhibited *B. cereus* and pure LIM inhibited *A. niger* and *P. variotii*. The presence of inhibition zones around the samples in these controls confirms the sensitivity of the microorganisms to the free substances.

Due to their hydrophobic nature, essential oils and their derivatives can interact with bacterial phospholipid membranes, causing structural damage, protein denaturation, and destabilization of enzymatic systems.[6,60] Similarly, these compounds exhibit antifungal activity through multiple mechanisms, including membrane and cell wall disorganization, inhibition of chitin and ergosterol synthesis, and morphological alterations in hyphae. Essential oils may also impair mitochondrial function, reducing ATP production and increasing reactive oxygen species (ROS), which directly affects fungal growth and viability.[71] Studies have further demonstrated the antimicrobial activity of PLM when incorporated into polymer matrices, inhibiting bacteria such as *Staphylococcus aureus*,[5] *Escherichia coli*,[46] *Clostridium perfringens*, *Pseudomonas aeruginosa* and *B. cereus*.[11] For fungi, PLM showed activity against *Colletotrichum gloeosporioides*[11] and *A. niger*.[46] Comparable results have been described for citrus essential oils rich in LIM against species such as *Aspergillus flavus*, *Penicillium verrucosum* and *Penicillium chrysogenum*.[72]

In this context, the lack of antimicrobial activity in films containing LIM and PLM may be attributed to the low concentrations of additives used (2.5% and 5.0%). This explanation is consistent with previous studies that achieved antimicrobial effects using concentrations above 10% in various polymer matrices.[5,46] Additionally, as shown in Fig. 8, pure LIM exhibited notable antifungal activity against the tested species. This suggests that the compound is indeed bioactive against fungi, provided that adequate concentrations are used.

Therefore, higher concentrations of LIM and PLM may be necessary to promote significant antimicrobial properties in SA-based films. These findings emphasize the importance of further studies to optimize formulation and incorporation methods, supporting the potential of terpenes and their derivates for active packaging applications in the food industry.

3.11 Economic and application perspectives of poly(limonene) synthesis

The photopolymerization of LIM is a relatively recent methodology, with most studies currently focused on laboratory-scale production. One of the main limitations for large-scale implementation is the relatively low monomer conversion and oligomer yield reported to date,[33] which require further optimization in terms of reaction kinetics, photoinitiating systems, and reactor design.

Although a detailed techno-economic assessment of the LIM photopolymerization pathway is still lacking, recent studies on LIM-derived polymers, particularly poly(limonene carbonate), have reported production costs comparable to fossil-based polymers (1.36–1.51 USD kg^{-1}), such as polystyrene. These studies provide the most comprehensive economic data currently available for LIM-based materials. Importantly, they indicate that upstream processing steps, such as LIM extraction and oxidation, dominate the economic and environmental costs.[73] This suggests that the polymerization step itself, including photopolymerization routes, may not represent the primary cost barrier. In this context, light-induced synthesis is particularly promising for industrial scaling, as it combines high process efficiency with low energy consumption and reduced operational costs.[74,75] These features indicate that the photopolymerization pathway has the potential to be economically viable, especially when integrated with optimized upstream limonene production. Therefore, while the present methodology still requires further optimization, it offers competitive prospects for future scale-up scenarios.

From an application perspective, PLM synthesis represents an alternative strategy to conventional encapsulation

techniques used to reduce the volatility of essential oils.[5] While encapsulation approaches, such as those based on nanoparticle carriers or chemical crosslinking, often provide high loading capacity and controlled release properties, they typically involve multi-step processing and complex formulations.[76] Specifically, when compared to alginate/collagen systems crosslinked with EDC/NHS reported for antimicrobial applications,[77] the present approach offers advantages particularly relevant to food packaging applications.

Although EDC/NHS crosslinking is highly effective for developing stable nanocarriers in biomedical contexts, its use is often associated with relatively high reagent costs and the requirement for multi-stage processing, including strict pH control and subsequent purification steps.[77] In contrast, the photopolymerization of LIM is a relatively simple process conducted under mild conditions, avoiding the need for specialized crosslinkers. Furthermore, the resulting PLM exhibits significantly lower volatility and improved thermal stability than its precursor monomer.[11,33] Overall, this strategy aligns with current trends toward renewable and food-safe materials, offering a more straightforward and potentially scalable route for the development of active biodegradable packaging films.

4 Conclusions

The synthesis of PLM as a thermally more stable oligomer compared to LIM was successful, as was its incorporation into SA-based films. SEM images revealed a homogeneous surface distribution of the oligomer within the films, along with signs of terpene detachment from the polymer matrix. Visual and color analysis of the films confirmed an intensified yellow coloration in the active films containing PLM. FT-IR spectra showed a reduction in the hydroxyl band in the additive-containing samples. The addition of these active compounds also decreased the crystallinity of the films but slightly improved their thermal stability and mechanical properties. PLM-containing films exhibited higher tensile strength and flexibility compared to the control and LIM-containing films, reaching tensile strength values as high as 46 $\pm$ 5 MPa and an elongation at break of 14 $\pm$ 5%. The film-forming solutions of all tested formulations did not exhibit antimicrobial activity, likely due to the low concentrations of the additives used, even though the pure terpene demonstrated inhibitory effects against the tested microorganisms. Although reductions in moisture content and water vapor permeability were not statistically significant, these improvements suggest the functional potential of the additives, even at reduced concentrations. Finally, PLM enhanced the antioxidant and light barrier properties of the SA films, reaching values of 7.8 $\pm$ 0.7% DPPH scavenging, 77 $\pm$ 16% ABTS scavenging, and 95.5 $\pm$ 0.5% total UV blocking efficiency. These results surpassed those observed for its monomer, reinforcing its suitability for active, biodegradable packaging systems. Taken together, these findings go beyond the simple characterization of LIM and PLM in SA films. By directly comparing a volatile terpene with its more stable oligomeric derivative, this study addresses a clear research gap. It also provides new insight into how molecular structure influences the multifunctionality of active films. In doing so, it contributes to the development of more stable, effective, and sustainable packaging materials.

Author contributions

M. M. Leonetti: formal analysis, investigation, data curation, writing – original draft, and visualization. V. E. de S. Gomes: formal analysis, investigation, and writing – review & editing; G. F. Schutz: formal analysis, investigation, and writing – review & editing; L. A. G. A. da Silva: formal analysis, investigation, and writing – review & editing; L. de O. Rocha: methodology, resources, and writing – review & editing; R. P. Vieira: methodology, validation, resources, and writing – review & editing; L. Marangoni Júnior: conceptualization, methodology, validation, resources, writing – review & editing, supervision, project administration, and funding acquisition.

Conflicts of interest

The authors have nothing to declare.

Data availability

The data will be made available upon request.

Acknowledgements

This study was partly funded by the Coordination for the Improvement of Higher Education Personnel – Brazil (CAPES) – Financial Code 001. The authors would like to thank the Fundo de Apoio ao Ensino, Pesquisa e Extensão – FAEPEX of UNICAMP for the Early Career Grant No. 2978/24 and PIND No. 2519/25. Additionally, this study received partial financial support from the National Council for Scientific and Technological Development (CNPq), grant numbers 301184/2025-9 and 444408/2024-0. We acknowledge the support of the São Paulo Research Foundation (FAPESP) [Grant number 2022/02728-0, 2024/07891-2 and 2024/07555-2].

References

1 Jyoti, A. K. Gupta, A. Kumar and B. Kumar, *Trends Food Sci. Technol.*, 2025, **163**, 105148.
2 D. R. Adhika, G. Genecya, A. A. Habibah, A. N. A. R. Putri and U. S. F. Arrozi, *OpenNano*, 2025, **22**, 100234.
3 M. Zhao, P. Han, H. Mu, S. Sun, J. Dong, J. Sun, S. Lu, Q. Wang and H. Ji, *Food Chemistry: X*, 2025, **25**, 102174.
4 T. F. Santos, C. M. Santos, H. J. Rao, M. R. Sanjay, J. H. O. Nascimento, D. F. S. Souza, F. Gapsari, R. Raharjo and S. Siengchin, *Food Chem. Adv.*, 2025, **6**, 100936.
5 J. V. Santana, L. Marangoni Júnior, G. Z. Cassol, H. H. Sato and R. P. Vieira, *Food Hydrocoll.*, 2024, **149**, 109558.
6 M. H. R. Barbosa, S. d. Á. Gonçalves, L. Marangoni Júnior, R. M. V. Alves and R. P. Vieira, *J. Food Meas. Char.*, 2022, **16**, 2011–2023.

7 S. d. Á. Gonçalves, M. H. R. Barbosa, L. Marangoni Júnior, R. M. V. Alves and R. P. Vieira, *Food Packag. Shelf Life*, 2023, **37**, 101085.
8 F. N. Eze, T. J. Jayeoye, R. C. Eze and C. Ovatlarnporn, *Int. J. Biol. Macromol.*, 2024, **255**, 128073.
9 H. Zhu, S. Chen, J. Xue, X. Wang, T. Yang, J. He and Y. Luo, *Int. J. Biol. Macromol.*, 2025, **297**, 139762.
10 T. C. Vianna, C. O. Marinho, L. Marangoni Júnior, R. M. V. Alves, L. H. I. Mei, C. C. Tadini and R. P. Vieira, *Waste Biomass Valoriz.*, 2023, **14**, 3133–3145.
11 T. C. Vianna, S. d. Á. Gonçalves, L. Marangoni Júnior, R. M. V. Alves, V. T. Andrade, H. H. Sato and R. P. Vieira, *ACS Sustain. Chem. Eng.*, 2024, **12**, 8752–8764.
12 L. Marangoni Júnior, P. R. Rodrigues, E. Jamróz, R. G. da Silva, R. M. V. Alves and R. P. Vieira, *J. Polym. Environ.*, 2023, **31**, 1853–1865.
13 M. Akbar, A. Yaqoob, A. Ahmad and R. Luque, *Sodium Alginate-Based Nanomaterials for Wastewater Treatment*, Elsevier, 2022, pp. 1–17.
14 N. M. Sanchez-Ballester, B. Bataille and I. Soulairol, *Carbohydr. Polym.*, 2021, **270**, 118399.
15 P. Yan, W. Lan and J. Xie, *Trends Food Sci. Technol.*, 2024, **143**, 104217.
16 V. U. Siddiqui, R. A. Ilyas, S. M. Sapuan, N. H. A. Hamid, P. S. Khoo, A. Chowdhury, M. S. N. Atikah, M. S. A. Rani and M. R. M. Asyraf, *Int. J. Biol. Macromol.*, 2025, **298**, 139946.
17 E. M. Hia, I. W. Suh, S. R. Jang and C. H. Park, *Carbohydr. Polym.*, 2024, **346**, 122666.
18 R. Priyadarshi, S. Roy, T. Ghosh, D. Biswas and J. W. Rhim, *Sustainable Mater. Technol.*, 2022, **32**, e00353.
19 K. Ma, F. Li, T. Zhe, X. Sun, X. Zhang, P. Wan, H. Na, J. Zhao and L. Wang, *Food Chem.*, 2024, **435**, 137552.
20 H. Baishya and S. Kumar, *Trends Food Sci. Technol.*, 2025, **161**, 105042.
21 H. Xiaowei, Z. Wanying, Z. Ke, S. Jiyong, Z. Xiaodong, Z. Junjun, S. Tingting, L. Hongcheng, L. Tao, Z. Xiaobo and L. Zhihua, *Int. J. Biol. Macromol.*, 2025, **318**, 145227.
22 M. Kashiri, *Appl. Food Res.*, 2025, 101051.
23 S. Sharma, S. Barkauskaite, A. K. Jaiswal and S. Jaiswal, *Food Chem.*, 2021, **343**, 128403.
24 T. C. Vianna, C. O. Marinho, L. Marangoni Júnior, S. A. Ibrahim and R. P. Vieira, *Int. J. Biol. Macromol.*, 2021, **182**, 1803–1819.
25 O. L. Orhotohwo, P. Lucci, L. Aquilanti, A. K. Jaiswal, D. Pacetti and S. Jaiswal, *LWT*, 2025, **226**, 117960.
26 L. Mao, Z. Dong, F. Dong, X. Dai and Z. Cao, *Int. J. Biol. Macromol.*, 2025, **296**, 139738.
27 Q. Liang, P. Cao, H. Lu, Y. Du, L. Kang, H. Ma and X. Ren, *Int. J. Biol. Macromol.*, 2025, **315**, 144268.
28 W. Y. Tong, A. R. Ahmad Rafiee, C. R. Leong, W.-N. Tan, D. J. Dailin, Z. M. Almarhoon, M. Shelkh, A. Nawaz and L. F. Chuah, *Chemosphere*, 2023, **336**, 139212.
29 P. F. Onyekere, D. O. Nnamani, C. O. Peculiar-Onyekere and P. F. Uzor, *Green sustainable process for chemical and environmental engineering and science: plant-derived green solvents: properties and applications*, Elsevier, 2020, pp. 219–227.
30 M. Bacanli, A. A. Başaran and N. Başaran, *Polyphenols: prevention and treatment of human disease*, Elsevier, 2018, pp. 419–424.
31 E. Fortunati, F. Luzi, D. Puglia, F. Dominici, C. Santulli, J. M. Kenny and L. Torre, *Eur. Polym. J.*, 2014, **56**, 77–91.
32 H. C. Pan and S. Polat, *Ind. Crops Prod.*, 2023, **204**, 117308.
33 E. R. M. de Oliveira and R. P. Vieira, *J. Polym. Environ.*, 2020, **28**, 2931–2938.
34 L. Marangoni Júnior, R. G. da Silva, C. A. R. Anjos, R. P. Vieira and R. M. V. Alves, *Carbohydr. Polym.*, 2021, **269**, 118286.
35 G. Simon Maia, G. Ferreira Toledo, G. Frey Schütz, L. Marangoni Júnior and R. Pioli Vieira, *Int. J. Biol. Macromol.*, 2025, **319**, 145710.
36 L. Kang, Q. Liang, H. Chen, Q. Zhou, Z. Chi, A. Rashid, H. Ma and X. Ren, *Food Chem.*, 2023, **402**, 134237.
37 G. F. Schutz, R. M. V. Alves, C. Delarmelina, M. C. T. Duarte and R. P. Vieira, *Int. J. Biol. Macromol.*, 2024, **260**, 129482.
38 ASTM International, 2022, DOI: 10.1520/E0096_E0096M-22.
39 International Organization for Standardization, *Plastics—film and sheeting—determination of thickness by mechanical scanning*, Geneva, 1993.
40 ASTM-D882, 2018, preprint.
41 ASTM International, 2022, DOI: 10.1520/E1348-22.
42 B. Akachat, L. Himed, M. Salah, M. D'Elia, L. Rastrelli and M. Barkat, *Foods*, 2025, **14**, 353.
43 J. Jovanovic, V. F. M. Ornelis, A. Madder and A. Rajkovic, *Compr. Rev. Food Sci. Food Saf.*, 2021, **20**, 3719–3761.
44 T. van den Brule, M. Punt, W. Teertstra, J. Houbraken, H. Wösten and J. Dijksterhuis, *Environ. Microbiol.*, 2020, **22**, 986–999.
45 M. Ijadpanahsaravi, L. B. Snoek, W. R. Teertstra and H. A. B. Wösten, *Int. J. Food Microbiol.*, 2024, **410**, 110495.
46 G. F. Toledo, G. F. Schutz, L. Marangoni Júnior and R. P. Vieira, *Sustain. Mater. Technol.*, 2024, **41**, e011099.
47 X. Dang, S. Han, Y. Du, Y. Fei, B. Guo and X. Wang, *Food Chem.*, 2025, **466**, 142192.
48 L. Marangoni Júnior, E. Jamróz, S. de Á. Gonçalves, R. G. da Silva, R. M. V. Alves and R. P. Vieira, *Food Hydrocolloids Health*, 2022, 100094, DOI: 10.1016/j.fhfh.2022.100094.
49 H. Wang, M. Li, R. Ren, Z. Gao, L. Meng, Z. Li and C. Cao, *Carbohydr. Polym.*, 2025, 123430, DOI: 10.1016/j.carbpol.2025.123430.
50 U. Siripatrawan and W. Vitchayakitti, *Food Hydrocoll.*, 2016, **61**, 695–702.
51 P. Jegajeevanram, P. K. Abhilash, P. Gayathri, M. Abdur Rahman, N. Manikandan and P. Arulselvan, *Inorg. Chem. Commun.*, 2024, 113247, DOI: 10.1016/j.inoche.2024.113247.
52 P. Kumari, V. Kant and M. Ahuja, *J. Drug Deliv. Sci. Technol.*, 2024, 105451, DOI: 10.1016/j.jddst.2024.105451.
53 M. Younis, R. M. Kamel, A. Alhamdan, E. E. Fadly, A. I. Zein El-Abedein and M. N. Saleh, *Int. J. Biol. Macromol.*, 2025, 143058, DOI: 10.1016/j.ijbiomac.2025.143058.
54 J. Lv, P. Chen and P. Li, *Int. J. Biol. Macromol.*, 2025, 144370.
55 S. Tanaka, A. Doi, N. Nakatani, Y. Katayama and Y. Miyake, *Carbon*, 2009, **47**, 2688–2698.
56 E. Kinnertová, T. Zelenka, G. Zelenková, L. Kořená, V. Slovák and M. Almáši, *Carbon Trends*, 2024, **17**, 100401.

57 N. T. Nguyen, V. T. Nguyen, T. T. Vu, T. V. Le Nguyen, T. T. T. Nguyen, P. D. Huynh, B. A. Pham, N. Q. Tran, D. T. Nguyen and P. Le Thi, *Macromol. Res.*, 2024, **32**, 427–442.
58 J. Long, W. Zhang, M. Zhao and C.-Q. Ruan, *Carbohydr. Polym.*, 2023, **321**, 121267.
59 Y. Li, C. Tang and Q. He, *Food Biosci.*, 2021, **41**, 100927.
60 L. Atarés and A. Chiralt, *Trends Food Sci. Technol.*, 2016, **48**, 51–62.
61 J. Criollo-Feijoo, V. Salas-Gomez, F. Cornejo, R. Auras and R. Salazar, *Heliyon*, 2024, **10**, e36150.
62 G. S. Lemos, J. S. Vitoria, L. M. Fonseca, J. B. Pires, F. T. da Silva, T. J. Siebeneichler, C. d. O. Pacheco, E. A. Gandra and E. d. R. Zavareze, *Int. J. Biol. Macromol.*, 2025, **310**, 143441.
63 A. Tenorio-Alfonso, E. Vázquez Ramos, I. Martínez, M. Ambrosi and M. Raudino, *J. Mech. Behav. Biomed. Mater.*, 2023, **139**, 105668.
64 M. Alizadeh Sani, A. Khezerlou, M. Tavassoli, A. H. Abedini and D. J. McClements, *Trends Food Sci. Technol.*, 2024, **145**, 104366.
65 M. He, Y. Huang, X. Zhang, W. Zhu, W. Shao, J. Wang, D. Xu and W. Yao, *Int. J. Biol. Macromol.*, 2024, 130821, DOI: 10.1016/j.ijbiomac.2024.130821.
66 R. He, X. Wang, P. Chen, M. He and H. Qi, *Int. J. Biol. Macromol.*, 2024, 138170, DOI: 10.1016/j.ijbiomac.2024.138170.
67 B. Rukmanikrishnan, S. K. Rajasekharan, J. Lee, S. Ramalingam and J. Lee, *Mater. Today Commun.*, 2020, **24**, 101346.
68 B. Rukmanikrishnan, F. R. M. Ismail, R. K. Manoharan, S. S. Kim and J. Lee, *Int. J. Biol. Macromol.*, 2020, **148**, 1182–1189.
69 S. Van Nguyen and B.-K. Lee, *Carbohydr. Polym.*, 2022, **298**, 120064.
70 X. Dang, S. Han and X. Wang, *J. Colloid Interface Sci.*, 2025, **694**, 137698.
71 F. Nazzaro, F. Fratianni, R. Coppola and V. De Feo, *Pharmaceuticals*, 2017, **10**, 86.
72 M. Viuda-Martos, Y. Ruiz-Navajas, J. Fernández-López and J. Pérez-Álvarez, *Food Control*, 2008, **19**, 1130–1138.
73 M. T. Bertão and R. P. Vieira, *ACS Polym. Au*, 2026, DOI: 10.1021/acspolymersau.5c00192.
74 D. Czachor-Jadacka and B. Pilch-Pitera, *Prog. Org. Coat.*, 2021, **158**, 106355.
75 Y. Ji, C. Zhang, X. Xu, J. Zhao, J. Liu and Y. Huo, *Small*, 2025, **21**, e09388.
76 D. R. Reis, A. Ambrosi and M. Di Luccio, *Future Foods*, 2022, **5**, 100126.
77 F. S. G. T. Valookolaei, H. Sazegar and L. Rouhi, *BMC Biotechnol.*, 2024, **24**, 86.